Pharmaceutical Research, Vol. 27, No. 4, April 2010 (© 2010)
DOI: 10.1007/s11095-009-0016-y

Research Paper

Hepatic Disposition of Ximelagatran and Its Metabolites in Pig; Prediction of the Impact of Membrane Transporters Through a Simple Disposition Model

Erik Sjögren,[1] Ulf Bredberg,[2] Erik Allard,[3] Björn Arvidsson,[3,4] Jonas Bergquist,[3] Tommy B. Andersson,[5,6] and Hans Lennernäs[1,7]

Received August 19, 2009; accepted November 20, 2009; published online February 6, 2010

Purpose. The double prodrug, ximelagatran, is bioconverted, via the intermediates ethylmelagatran and N-hydroxymelagatran, to the direct thrombin inhibitor, melagatran. The primary aim of this study was to investigate the hepatic metabolism and disposition of ximelagatran and the intermediates in pig. A secondary aim was to explore a simple *in vitro* methodology for quantitative investigations of the impact of membrane transporters on the disposition of metabolized drugs.
Methods. Porcine S1 (supernatant fraction obtained by centrifuging at 1,000 g for 10 min) liver fractions and hepatocytes were incubated in the absence and presence of known membrane transporter inhibitors. The *in vitro* kinetics and disposition were determined by simultaneously fitting the disappearance of ximelagatran and the appearance of the metabolites.
Results. In S1 liver fractions, the metabolism was significantly inhibited by co-incubation of verapamil or ketoconazole, but not by erythromycin, quinine or quinidine. The disposition of ximelagatran and the intermediate metabolites in hepatocytes were influenced, to various degrees, by carrier-mediated transport processes.
Conclusion. This work demonstrates that it is possible to obtain profound information on the general mechanisms that are important in the drug liver disposition using the combination of common *in vitro* systems and the simple disposition model proposed in this study.

KEY WORDS: hepatic disposition; hepatocytes; kinetic modeling; melagatran; prodrug.

INTRODUCTION

Melagatran (MEL) is a novel, direct thrombin inhibitor for the prevention and treatment of thromboembolic disorders (1,2). Unfortunately, MEL is associated with hepatotoxicity and was withdrawn from the market in 2006 (3,4). To improve the poor and variable bioavailability of MEL, caused by low membrane permeability, a double prodrug, ximelagatran (XIM), was developed (5,6). XIM includes an ethyl ester and an N-hydroxylated amidine in place of the carboxylic acid and amidine groups on MEL. Following oral administration, XIM is rapidly and extensively absorbed (>80% in pigs) and bioconverted to MEL through hydrolysis of the ethyl group—mediated by carboxylesterases—and reduction of the hydroxyl group—catalyzed by a three component system including cytochrome β, its reductase and a third unidentified protein (7–9). These sequential reactions can take place through two different pathways involving two intermediate metabolites: ethylmelagatran (ETM) and N-hydroxymelagatran (OHM) (Fig. 1). *In vitro* and *in vivo* investigations have shown that neither XIM nor its metabolites are substrates or inhibitors of cytochrome P450 (CYP) isoenzymes (10). However, recent non-clinical and clinical studies have shown an increase in MEL plasma exposure when co-administered with erythromycin (7,11). This drug-drug interaction has been proposed to reduce biliary excretion of XIM and MEL by inhibiting active transport mediated by P-glycoprotein (P-gp, MDR1, *ABCB1*)

Electronic supplementary material The online version of this article (doi:10.1007/s11095-009-0016-y) contains supplementary material, which is available to authorized users.

[1] Department of Pharmacy, Uppsala University, Box 580, 751 23 Uppsala, Sweden.
[2] Discovery DMPK & Bioanalytical Chemistry, AstraZeneca R&D, Mölndal, Sweden.
[3] Analytical Chemistry, Department of Physical and Analytical Chemistry, Uppsala University, Uppsala, Sweden.
[4] FOI, Swedish Defence Research Agency, CBRN Defence and Security, Umeå, Sweden.
[5] Clinical Pharmacology and DMPK, AstraZeneca R&D, Mölndal, Sweden.
[6] Section of Pharmacogenetics, Department of Physiology and Pharmacology, Karolinska Institutet, Stockholm, Sweden.
[7] To whom correspondence should be addressed. (e-mail: hans.lennernas@farmaci.uu.se)

ABBREVIATIONS: ACTB, β actin; BCRP, breast cancer resistance protein; C_u, unbound concentration; CYP, cytochrome P450; ETM, ethylmelagatran; f_u, fraction unbound; GAPDH, glyceraldehyde-3-phosphate dehydrogenase; HBSS, Hank's buffer salt solution; HPRT, hypoxanthine phosphoribosyltransferase; HSB, Hepatocyte suspension buffer; K_m, Michaelis constant; MEL, melagatran; MRP2, multi-drug resistance protein 2; NADH, reduced β-nicotinamide adenine dinucleotide; NADPH, reduced β-nicotinamide adenine dinucleotide phosphate; OHM, N-hydroxymelagatran; P-gp, P-glycoprotein; S1, supernatant fraction obtained by centrifuging at 1,000 g for 10 min; V_{max}, theoretical maximum reaction rate; XIM, ximelagatran.

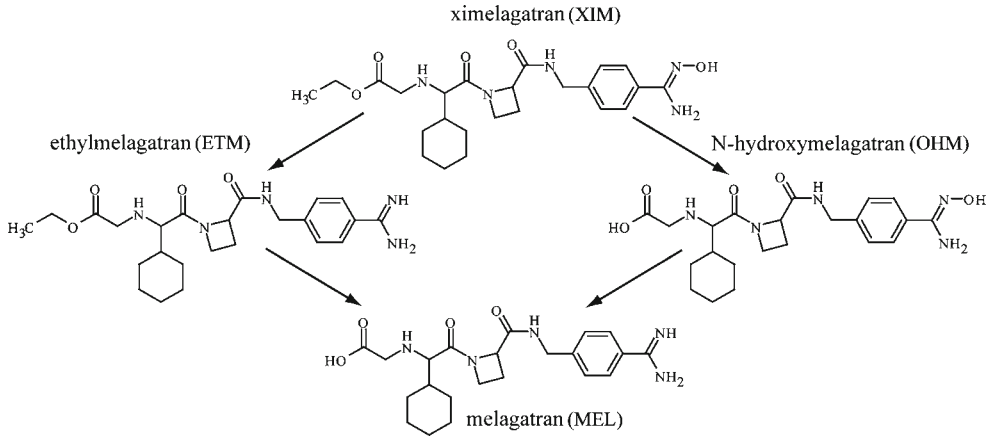

Fig. 1. The biotransformation of ximelagatran (XIM) via two intermediate metabolites, ethylmelagatran (ETM) and N-hydroxymelagatran (OHM), to melagatran (MEL).

(11). Similar results were reproduced in pigs, but although an overall decrease in biliary excretion was observed, this could not fully explain the increase of approximately 50% in exposure of MEL. Total excretion of XIM in bile following enteral administration decreased from 13% to 9.3%, of which the majority consisted of MEL and the intermediate metabolite, ETM. In addition, Sjödin *et al.* have demonstrated species-specific, route-dependent pharmacokinetic behavior most likely due to a significantly higher first-pass metabolism in the gut wall in pigs (7). Further, recent published *in vitro* data performed with porcine S1 (supernatant fraction obtained by centrifuging at 1,000 g for 10 min) liver fractions strongly indicate other significant, not yet identified, metabolic routes involved in the metabolism of OHM (12). The primary objective of this study was to investigate the metabolism of XIM and its intermediates in porcine S1 liver fractions and hepatocytes in the absence and presence of known membrane transporter inhibitors. A secondary aim was to explore a simple methodology, applicable to these *in vitro* systems, for quantitative investigations of the impact of membrane transporters on the disposition of metabolized drugs.

MATERIALS AND METHODS

Chemicals

XIM, ETM, OHM, MEL and respective isotopically labeled internal standards were provided by AstraZeneca (Mölndal, Sweden). Hank's buffer salt solution (HBSS) and L-glutamine were purchased from Invitrogen (Lidingö, Sweden). Collagenase A was acquired from Roche (Mannheim, Germany). Acetonitrile, methanol and ammonium acetate of analytical grade were purchased from Merck (Darmstadt, Germany). Water was purified with a Milli-Q purification system (Millipore, Bedford, MA, USA). All other chemicals and reagents, including erythromycin, quinidine, quinine, verapamil, ketoconazole, Williams Medium E, trypsin inhibitor, HEPES, DNase I and EGTA were obtained from Sigma Aldrich Company Ltd. (Stockholm, Sweden). Hepatocyte suspension buffer (HSB) consisted of 2.8 g Na HEPES, 5 ml 7.5% (*w*/*v*) $NaHCO_3$, 200 ml HBSS 1X, 100 ml HBSS 10X diluted to a volume of 1,200 ml in water and adjusted to pH 7.4 with 1 M HCl and 1 M NaOH. Animal material 6–7-month-old male Swedish Landrace pigs) was collected at the local slaughter house.

Preparation of Porcine S1 Liver Fractions

Fresh porcine liver was flushed with ice-cold isotonic saline solution to remove blood and decrease tissue temperature. End lobe pieces of the liver were homogenized in ice-cold potassium phosphate buffer (0.1 M, pH 7.4) (1:5 *v*/*w*) with an ULTRA-TURRAX dispersion unit (IKA, Staufen, Germany) for 0.5 min at 6,500 rpm and then centrifuged at 1,000 g for 10 min. The supernatant was collected as the S1 fraction and used within 60 min to minimize the risk of enzymatic degradation and reduction in activity. Preparations were conducted on ice in a refrigerated room at 8°C, and S1 fractions were kept on ice until use. Total protein concentration was determined using a Quick Start Bradford kit (Bio-Rad Laboratories AB, Sundbyberg, Sweden) with immunoglobulin as reference protein.

Preparation of Porcine Hepatocytes

Isolation of porcine hepatocytes was performed using a modified version of the technique of digestion of biopsies using collagenase (13). Briefly, a liver biopsy was taken from an end lobe directly after the death of the animal and put into ice-cold saline solution for transportation to the laboratory. The isolation procedure was started within 20 min of collection. The liver biopsy was placed on a steel wire screen, and exposed blood vessels were cannulated with up to 4 cannulas. A wash-out perfusion was performed with HSB containing 0.5 mM EGTA for 7.5 min followed by a second wash-out perfusion with HSB for 10 min. This was followed by a digestion perfusion with HSB containing 5 mM $CaCl_2$, collagenase (150 CDU ml^{-1}) and trypsin inhibitor (700 BAEE ml^{-1}) until the biopsy showed evidence of extensive digestion (usually 15–20 min). All perfusions were performed with solutions heated to 37°C at a flow rate of 5 ml min^{-1} $cannula^{-1}$. The digested liver sample was then gently moved to a plastic petri dish filled with ice-cold HSB containing DNase (1600

Dornase ml^{-1}), and the hepatocytes were gently dissociated from the connective tissue. The suspension was filtered through nylon mesh, and the filtrate was washed in three repeated centrifugation (3 min at 25 g) and resuspension steps: the first in HSB containing DNase (1600 Dornase ml^{-1}) and the following two steps in HSB. All steps were performed with ice-cold media. The resulting pellet was resuspended in Williams' medium E (pH 7.4) containing 2 mM L-glutamine and 25 mM HEPES and the cell yield and viability were determined using a NucleoCounter (ChemoMetec, Allerød, Denmark). Inspection of the cell suspensions was made microscopically. Cell yield (on average 100×10^6 cells) was corrected to account for a 20% prevalence of cells with two cell nuclei. Only cell yields with a viability of >85% were used, and all experiments were conducted within 60 min of isolation.

RNA Isolation from Hepatic Tissue and Hepatocytes

Pooled tissue (n=4) and hepatocyte (n=2) samples were collected and used for RNA isolation. The samples were immediately submerged in RNAlater (Qiagen, Hilden, Germany), and after 12 h storage at 8°C, the RNA was isolated using an RNeasy mini kit (Qiagen, Hilden, Germany). Reverse transcription was performed using the cDNA High Capacity Archive kit (Applied Biosystems, Foster City, CA, USA). Real-time PCR was performed in a volume of 10 µl containing ~20 ng cDNA, 0.5 µM forward and reverse primers, and 5 µl DyNAmo Capillary SYBR Green qPCR solution (Finnzymes, Espoo, Finland). Porcine-specific primers for P-gp (*ABCB1*), multi-drug resistance protein 2 (MRP2, *ABCC2*), breast cancer resistance protein (BCRP, *ABCG2*), glyceraldehyde-3-phosphate dehydrogenase (GAPDH), β actin (ACTB) and hypoxanthine phosphoribosyltransferase (HPRT) were used as described (14) and purchased from Isogen (Isogen Life Science, Maarssen, The Netherlands). PCR products were quantified fluorometrically using SYBR Green, and the relative expression level of each transporter protein was calculated. The following formula was used: relative expression = $2^{-\Delta C}$, where ΔC = (C (target gene)–C (housekeeping genes GAPDH, ACTB, HPRT)).

Incubations for Determination of Kinetics in S1 Liver Fractions

Incubations were conducted by shaking under air at 37°C. The incubation matrix consisted of potassium phosphate buffer (final concentration 0.1 M, pH 7.4) and porcine liver S1 fractions at a final concentration of 0.6 mg ml^{-1}. Incubations were also performed to investigate if the membrane transporter inhibitors under investigation in the subsequent hepatocyte experiment had any significant influence on metabolism. These experiments were performed by adding the inhibitors to the incubation matrix (verapamil (100 µM and 10 µM), ketoconazole (5 µM), erythromycin (50 µM), quinidine (50 µM) and quinine (50 µM)). Reduced β-nicotinamide adenine dinucleotide (NADH) and reduced β-nicotinamide adenine dinucleotide phosphate (NADPH) were added after 5 min preincubation to a final concentration of 1 mM, and after 2 min the reaction was started by adding XIM to a final concentration of 10 µM. Samples of 80 µl were removed at 0, 15, 30, 45, 60, 75, 90, 105 and 120 min for incubations excluding inhibitors and at 0, 60 and 120 min for incubations containing inhibitors (with the exception of incubations containing verapamil where samples were removed at 0, 30 and 60 min). The reactions were terminated by adding the samples to 100 µl ice-cold acetonitrile containing the internal standards. After termination, samples were centrifuged for 10 min at 10,000 g, and an aliquot of the supernatant was drawn and stored at –20°C until sample analysis. Formation of unidentified entities during the incubations were calculated by subtracting the sum of known compounds at given time points from the concentration of XIM at t=0. Incubations with S1 fractions inactivated by storage at RT for 48 h were carried out in parallel to check stability in incubation media. The fraction unbound in incubation ($f_{uinc.}$) was determined by ultrafiltration as described previously (12). Published values of f_{uinc} were used for ETM and OHM throughout the study (12).

Incubations for Determination of Kinetics in Hepatocytes

Incubations were conducted by shaking at 37°C under 5% CO_2. Porcine hepatocytes (final concentration 1×10^6 viable cells ml^{-1}) and Williams' medium E (pH 7.4) containing 2 mM L-glutamine and 25 mM HEPES with or without membrane transporter inhibitor (erythromycin, quinine and erythromycin + quinine at final concentrations of 50 µM) were preincubated for 5 min. The reaction was initiated by the addition of XIM to a final concentration of 10 µM. Samples of 80 µl were removed at 0, 15, 30, 45, 60, 75, 90, 105 and 120 min for incubations excluding inhibitors and at 0, 30, 60, 90 and 120 min for incubations containing inhibitors. Before removal of samples, incubation tubes were shaken to ensure that removed samples contained a homogeneous cell suspension, i.e. both media and cells. The reactions were terminated by adding the samples to 100 µl ice-cold acetonitrile containing the internal standards. After termination, samples were centrifuged for 10 min at 10,000 g, and an aliquot of the supernatant was drawn and stored at –20°C until sample analysis. Formation of unidentified entities during the incubations were calculated by subtracting the sum of known compounds at given time points from the concentration of XIM at t=0.

Sample Analysis

Samples were thawed and diluted 10-fold with water before analysis, using the method previously described by Arvidsson *et al.* (15). A refrigerated CMA microdialysis autosampler (CMA Microdialysis AB, Stockholm, Sweden) operating at 5°C was used for sample injection using a 5 µL loop. For sample trapping and analyte separation in house slurry packed fused silica capillaries (200 µm id) were used; C4 trap column (5 cm) and C18 analytical column (15 cm). Mobile phase A consisted of 10 mM ammonium acetate and 4.5 mM acetic acid, and mobile phase B consisted of 10 mM ammonium acetate, 4.5 mM acetic acid and 95% acetonitrile (v/v). The sample was loaded onto the trapping column using mobile phase A with a flow rate of 10 µL min^{-1}, followed by backflushing of the sample onto the analytical column. Gradient separation was performed using a flow rate of

5 μL min^{-1} delivered by a LC Packings Ultimate capillary HPLC systT (Amsterdam, The Netherlands). Mass spectrometry was performed on a PE Sciex API III + triple quadrupole mass spectrometer (PE Sciex, Concord, Canada) equipped with an electrospray ionization interface used in MRM mode with a dwell time set to 400 ms for each transition. The mass spectrometer was operated in positive ion mode with a spray potential set to 4,300 V, and the orifice potential was set to 35 V. Furthermore, the collision energy was set to 26 eV with a collision gas thickness of 200×10^{13} molecules cm^{-2}. Integration of peaks was performed with McQuan 1.3 software (PE Sciex, Concord, Canada). The lower limits of quantitation (with mean precision in RSD %) for XIM, ETM, OHM and MEL were 1.5 nM (4.2%), 3.6 nM (7.3%), 3.0 nM (5.0%) and 3.0 nM (6.5%), respectively.

Kinetics in S1 Liver Fractions

In vitro kinetics in S1 liver fractions were determined by simultaneously fitting of the disappearance of XIM and appearance of ETM, OHM and MEL (see supplemental data). Optimization of the kinetic model was performed by iterative incorporation of enzymatic instability and unidentified metabolic pathways. Previously reported enzyme kinetic data of ETM and OHM were fixed in the kinetic analysis performed in this study (12). In addition, to investigate non-linearity at present conditions, each independent pathway involved in the disappearance of XIM was tested for both linear kinetics (a reaction of the first order, Eq. 1) and non-linear kinetics (described by the Michaelis Menten equation, Eq. 2).

$$\frac{dC}{dt} = -C \times k_{met.S1} \times f_{uinc.} = v \tag{1}$$

where C is the concentration measured in the incubation, $k_{met.S1}$ represents the metabolic rate constant and $f_{uinc.}$ is the fraction unbound in the incubation.

$$\frac{dC}{dt} = -\frac{V_{\max} \times C \times f_{uinc.}}{K_m + (C \times f_{uinc.})} = v \tag{2}$$

where V_{max} and K_m represent the theoretical maximum reaction rate and the Michaelis constant, respectively.

The disappearance of ETM and OHM was always fitted to a model using Eq. 2. Enzymatic activity throughout the incubation period, for each individual reaction, was fitted to a model described as a monoexponential decay, (Eq. 3).

$$\frac{dC}{dt} = v \times e^{-k_{EAC} \times t} \tag{3}$$

where k_{EAC} is the rate constant describing the reduction in enzyme activity.

For ETM and OHM, values of k_{EAC} were fixed with previously published values (12).

Kinetics in Hepatocytes

Enzymatic depletion rate constants ($k_{met.hep}$) were scaled by multiplying the rate constants obtained from the S1 analysis (above) with the amount of protein per hepatocyte ($A_{prot.hep}$) divided by protein concentration in the S1 preparation ($C_{prot.S1}$) and the hepatocyte volume (V_{hep}) (Eq. 4).

$$k_{met.hep} = \frac{k_{met.S1}}{C_{prot.S1}} \times \frac{A_{prot.hep}}{V_{hep}} \tag{4}$$

$A_{prot.hep}$ was calculated from the protein concentration determined in the S1 fraction preparations, taking the dilution (1:5) into account, and a cell concentration of 120×10^6 hepatocytes per gram of liver (16,17). A hepatocyte volume of 5×10^{-9} ml per cell was assumed in this study based on prior published measurements (18–21).

The relations between total, intracellular and extracellular volume (V), amount (X) and concentration (C) in the incubation can be expressed as follows:

$$C_{tot} = \frac{X_e + X_i}{V_e + V_i} = \frac{X_i}{V_i} \times \frac{1 + \frac{X_e}{X_i}}{1 + \frac{V_e}{V_i}} = Ci \times \frac{1 + \frac{X_e}{X_i}}{1 + \frac{V_e}{V_i}} \tag{5}$$

where the subscripts *tot*, *e* and *i* denote total, extracellular and intracellular, respectively.

The relation between intra- and extracellular concentration at equilibrium can be described by a distribution constant (D) as follows:

$$C_e = \frac{C_i}{D} \rightarrow \frac{X_e}{V_e} = \frac{X_i}{D \times V_i} \rightarrow \frac{X_e}{X_i} = \frac{V_e}{D \times V_i} \tag{6}$$

where C_e and C_i are represented by the total amount of drug and volume of these compartments.

Inserting Eq. 6 in Eq. 5 gives:

$$C_{tot} = C_i \times \frac{\left(\frac{V_e}{D \times V_i}\right) + 1}{\frac{V_e}{V_i} + 1} \rightarrow C_i = C_{tot} \times \frac{\frac{V_e}{V_i} + 1}{\left(\frac{V_e}{D \times V_i}\right) + 1} \tag{7}$$

Equation 7 expresses the intracellular concentration through the total concentration measured in the incubation, the relation between extra- and intracellular volume and the distribution of drug in these volumes. The quotient V_e / V_i was calculated to a value of 199 in the present analysis. Theoretically, the rate of metabolism for the entire incubation can be derived from following equations (as it is assumed that only the free fraction of the intracellular drug is available for metabolism):

$$\frac{dX_e}{dt} = -C_e \times k_{e\rightarrow i} \times f_{u.med} \times V_e + C_i \times k_{i\rightarrow e} \times f_{u.cell} \times V_i \tag{8}$$

$$\frac{dX_i}{dt} = C_e \times k_{e\rightarrow i} \times f_{u.med} \times V_e - C_i \times k_{i\rightarrow e} \times f_{u.cell} \times V_i - C_i \times k_{met.hep} \times f_{u.cell} \times V_i \tag{9}$$

$$\frac{dX_{tot}}{dt} = \frac{dX_e}{dt} + \frac{dX_i}{dt} = -C_i \times k_{met.hep} \times f_{u.cell} \times V_i \tag{10}$$

$$\frac{dC_{tot}}{dt} = \frac{dX_{tot}}{dt \times V_{tot}} = -C_i \times k_{met.hep} \times f_{u.cell} \times \frac{V_i}{V_{tot}} \quad (11)$$

$$\frac{dC_{tot}}{dt} = -C_{tot} \times \frac{\frac{V_e}{V_i} + 1}{\left(\frac{V_e}{D \times V_i}\right) + 1} \times k_{met.hep} \times f_{u.cell} \times \frac{V_i}{V_{tot}} = v \quad (12)$$

where $k_{e\rightarrow i}$ represents the rate constant describing the flow from extracellular space to intracellular space, and $k_{i\rightarrow e}$ represents the rate constant describing the opposite flow. $f_{u.med}$ and $f_{u.cell}$ represent the extracellular and intracellular unbound fractions, respectively.

Equation 12 makes it possible to express the rate of disappearance using only measurements of the total concentration in the incubation (media + cells) even though it is the intracellular concentration that undergoes metabolism and hence determines the metabolic rate. As no valid determination of $f_{u.cell}$ could be obtained, the calculations were performed using a value of $f_{u.cell}$ equal to $f_{uinc.}$.

The possible loss of active hepatocytes over time was modeled as a monoexponential decay, described by the rate constant, k_{HAC}, in correspondence with the S1 fraction analysis.

When XIM is added (t=0) to the incubation medium, the intracellular concentration of XIM equals 0. To describe the time for the intracellular and extracellular concentration of XIM to reach pseudo-equilibrium, both a sigmoid function (Eq. 13) and a monoexponential increase (Eq. 14) were evaluated, giving the final equations:

$$\frac{dC_{tot}}{dt} = v \times \frac{t^h}{t50^h + t^h} \times e^{-k_{HAC} \times t} \quad (13)$$

where h is the Hill factor, $t50$ the time to reach 50% equilibrium and k_{HAC} the hepatocyte decay constant and

$$\frac{dC_{tot}}{dt} = v \times \left(1 - e^{-k_{lag} \times t}\right) \times e^{-k_{HAC} \times t} \quad (14)$$

where k_{lag} represent the equilibrium constant.

Statistical analyses were performed using a two-sided unequal variance t-test.

Simulations

Simulations with a two-compartment model were made to investigate if reasonable levels of efflux rates, compared to present elimination rate, could significantly influence the disposition of an intracellularly formed and metabolized compound. The model used for a double prodrug (proD), an intermediate metabolite (intM) and the end product (drugD) is displayed in Fig. 2. To facilitate the interpretation of results, the influx/efflux rate relation ($k_{e\rightarrow i}/k_{i\rightarrow e}$) for intM was set to 1, and proD was only allowed intracellular distribution. Efflux/elimination rate relations ($k_{i\rightarrow e}/k_{met.}$) of 10, 3, 1, 1/3, 0.1 were investigated for intM. To mimic the experimental conditions in this study, simulations were performed with the following values for each respective parameter: metabolic rate constant (k_{met}) = 0.018 min^{-1}, formation rate constant (k_{app}) = 0.023 min^{-1}, second metabolic pathway rate constant (k_{sec}) = 0.024 min^{-1}, incubation time = 120 min and extra/intra cellular volume ratio = 199. For evaluation purposes, control simulations without metabolism and without distribution parameters were performed for intM, representing the result of a total distribution of intM to the extracellular and intracellular spaces, respectively.

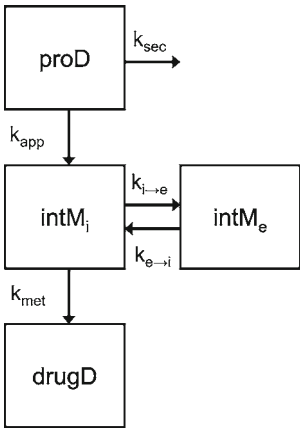

Fig. 2. Simple two-compartment model used to analyze effects of efflux of an intracellularly formed and metabolized intermediate metabolite. Indicated are the double prodrug (proD), the intermediate metabolite (intM), the active drug (drugD), the formation rate constant (k_{app}), efflux rate constant ($k_{i\rightarrow e}$), influx rate constant ($k_{e\rightarrow i}$), elimination rate constant (k_{met}) and second metabolic pathway rate constant (k_{sec}).

Data Analysis

Akaike information criterion, visual examination of data, residual plots and the precision of parameter estimation were used to evaluate and compare the goodness of fit for the different models. All analyses of kinetic data were performed using WinNonlin Professional software v4.0 (Pharsight Corp., CA, USA). Simulations were performed with Berkeley Madonna software v8.0.1 (University of California, Berkeley, CA, USA).

RESULTS

Kinetics in S1 Liver Fractions

Primary data from the control incubation in S1 liver fractions are displayed in Fig. 3, and final kinetic parameters are shown in Table I. Fraction XIM unbound in S1 liver fractions (f_{uinc}) was experimentally determined to 0.93. The final kinetic model best describing the biotransformation of XIM and its metabolites included two additional processes to the originally suggested metabolic outline (see supplemental data). Theoretically, these processes could be the sum of several unknown pathways, but as no discrimination of any such pathways was possible, they were regarded and modeled as single metabolic routes. The contribution of these processes to total disappearance was 26% for XIM and 78% for OHM, as previously described (12). Non-linear kinetics could not be applied to any of the metabolic routes involved in XIM

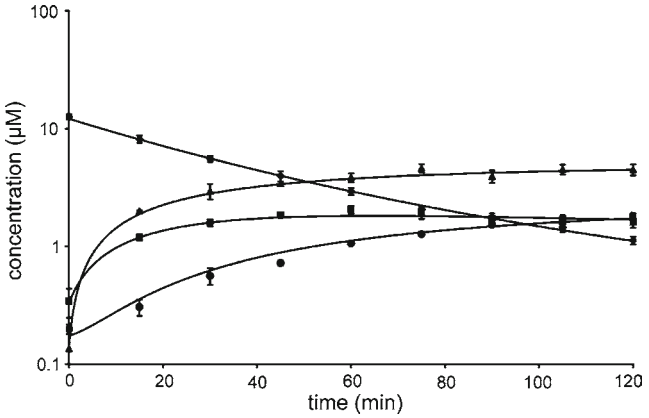

Fig. 3. Concentration-time profiles of ximelagatran (*diamonds*), ethylmelagatran (*squares*), N-hydroxymelagatran (*triangles*) and melagatran (*circles*) from the control experiment in S1 liver fractions. Mean ± S.D. (n=3) and final kinetic model fitted curves are displayed.

biotransformation, and, consequently, all reactions were expressed as monoexponential decays (Eq. 1). In addition, the data did not provide enough information to discriminate any differences in enzymatic instability for the different routes involved in XIM metabolism. Hence, the same rate constant for enzyme activity reduction was applied to all reactions. During the incubation period of 120 min, 91±0.7% of XIM was consumed and 13±0.5% MEL was formed. Further, 35±4% and 10±1% was recovered as OHM and ETM, respectively, while 32±3% was converted to unidentified metabolites. Impurities in XIM provided for the experiments were the sources of the concentrations for OHM, ETM and MEL at t=0.

Data from incubations including inhibitors were inadequate for kinetic modeling analysis. Hence, the assessment of potential inhibition was performed by comparing total turnover with or without inhibitors (Table II). Verapamil was detected as a potent inhibitor of the ester moiety cleavage in these incubations as both concentrations investigated almost completely prevented the formation of OHM (24% and 3% of the control value at 10 and 100 μM, respectively) and MEL (6.8% and 2.3% of the control value at 10 and 100 μM, respectively). Ketoconazole also significantly inhibited the formation of OHM (30% of the control value). The biotransformation of XIM and its metabolites was not affected by erythromycin or quinine. There were no major overall differences in recovered mass for inhibitor incubations compared to the control incubation. However, complete mass balance was obtained after co-incubations with verapamil (Table II).

Kinetics in Hepatocytes

Primary data from hepatocyte incubations are displayed in Fig. 4, and final kinetic parameters are shown in Table I. Microscopic inspection of the cell suspension revealed the presence of singles, pairs and clusters (n<10) of hepatocytes. The final kinetic model best describing the metabolism included a sigmoid lag function (Eq. 13) (h=1.26, t_{50}= 108 min) and a monoexponential hepatocyte activity decay (k_{HAC}=0.0158×min^{-1}). The distribution parameters (D, see Eq. 12) for XIM and ETM were calculated to be 3.0±0.2 and 1.8±0.1, respectively, but could not be reliably determined for OHM (0.001±0.07). During the incubation period of 120 min, 82±3% of XIM was consumed and 11±0.4% MEL was formed. In addition, 42±1% and 7.2±1% were recovered as OHM and ETM, respectively, and 22±3% was converted to unidentified metabolites. Impurities in XIM provided for the experiments were the sources of the concentrations for OHM, ETM and MEL at t=0.

Co-incubation of erythromycin increased the intracellular distribution of ETM 3.4-fold but did not significantly effect the distribution of XIM or OHM (Table I). Quinine decreased the intracellular distribution of XIM by 20% but increased intracellular distribution of ETM (2.7-fold) and OHM, making a reliable determination of the distribution constant of OHM possible (0.34±0.1). Co-incubation of both erythromycin and quinine increased the intracellular distribution of XIM and ETM but had no effect on OHM. These observations suggest that both cellular influx and efflux processes, mediated by one or several transporters, were affected. During the incubation period with erythromycin, quinine and a combination of both inhibitors, approximately 29±1%, 18±6% and 14±5% were converted to unidentified products, respectively. The disposition analyses including inhibitors were performed using parameter values for t_{50},

Table I. Summary of Kinetic Variables Obtained from Porcine S1 Liver Fractions, Metabolic Rate Constants ($k_{met,S1}$), and Porcine Hepatocyte Suspension, Distribution Constants (D)

S1 liver fractions			
	XIM → ETM	XIM → OHM	XIM → no ID
$k_{met,S1}$ (min^{-1})×10^3	11.6±0.58	22.8±1.1	12.6±2.6
Hepatocytes			
	D_{XIM}	D_{ETM}	D_{OHM}
CTRL	3.02±0.15	1.89±0.10	0.00100±0.071[a]
ERY	3.36±0.27	6.43±0.46**	0.00102±0.13[a]
QIN	2.52±0.19*	5.01±0.32**	0.343±0.12*
ERY + QIN	1.95±0.20**	5.42±0.41**	0.00440±0.11[a]

Values are shown as means with SE. Ximelagatran (XIM), ethylmelagatran (ETM), N-hydroxymelagatran (OHM), melagatran (MEL), Control incubation (CTRL), erythromycin 50 μM (ERY), quinine 50 μM (QIN) and erythromycin 50 μM + quinine 50 μM (ERY-QIN)
*p<0.05; **p<0.01
[a] Uncertain

Table II. Assessment of Investigated Membrane Transporter Inhibitors Effect on the Metabolic Processes Involved in Ximelagatrans Biotransformation in S1 Liver Fractions

	XIM		ETM		OHM		MEL		recovered mass	
	60 min	120 min	60 min	120 min	60 min	120 min	60 min	120 min	60 min	120 min
CTRL	23±1.6	8.9±0.7	14±1.3	10±1.4	29±2.6	35±3.9	6.8±0.25	13±0.51	73±3.3	66±4.2
ERY	30±2.3	12±0.31	10±0.61	7.6±0.58	34±2.9	39±7.2	5.6±0.79	12±1.1	80±3.8	72±7.3
QIN	32±3.1	14±1.9	13±1.0	11±0.58	33±7.3	36±1.7	5.8±0.54	12±0.77	83±8.0	73±2.8
ERY + QIN	33±3.7	16±1.3	12±2.3	12±1.5	29±3.0	38±4.9	5.3±0.81	11±0.86	79±5.4	77±5.4
QID	37±1.7	16±1.1	5.9±0.93	7.7±0.32	28±2.4	35±3.2	5.2±0.46	12±0.77	76±3.1	71±3.4
KET	47±0.47	23±2.5	7.9±0.27	8.9±1.7	9.5±2.1	11±2.8	4.0±0.14	9.9±0.65	68±2.2	52±4.2
VER10	87±1.0	n.a.	11±0.56	n.a.	7.3±0.19	n.a.	0.46±0.045	n.a.	106±1.2	n.a.
VER100	79±7.3	n.a.	23±2.1	n.a.	0.92±0.12	n.a.	0.16±0.056	n.a.	103±7.6	n.a.

Relative concentrations of ximelagatran (XIM), ethylmelagatran (ETM), N-hydroxymelagatran (OHM) and melagatran (MEL), as well as recovered mass, i.e. the sum of known compounds at given time points, presented as percent of initial ximelagatran concentration (mean ± S.D. (n=3)), after 60 and 120 min of incubation. Control incubation (CTRL), erythromycin 50 μM (ERY), quinine 50 μM (QIN), erythromycin 50 μM + quinine 50 μM (ERY-QIN), quinidine 50 μM (QID), ketoconazole 5 μM (KET), verapamil 10 μM (VER10), verapamil 100 μM (VER100). Data not available (n.a.)

and k_{HAC} determined in the control experiment as data were inadequate for modeling t_{50}, and hepatocyte activity was assumed to remain unaffected.

RNA Analysis

The relative expression of MRP2 RNA in hepatocytes and liver tissue samples was 10±0.4 and 7.2±0.1, respectively. The relative expression of P-gp was 1.0±0.1 in hepatocytes and 0.36±0.06 in liver tissue samples. Expression of BCRP was detected in neither hepatocytes nor liver tissue samples. Only GAPDH was used to calculate relative expression as both ACTB and HPRT were highly variable between samples.

Simulations

Results from the compartmental kinetic simulation study are displayed in Table III and Fig. 5. The simulations showed

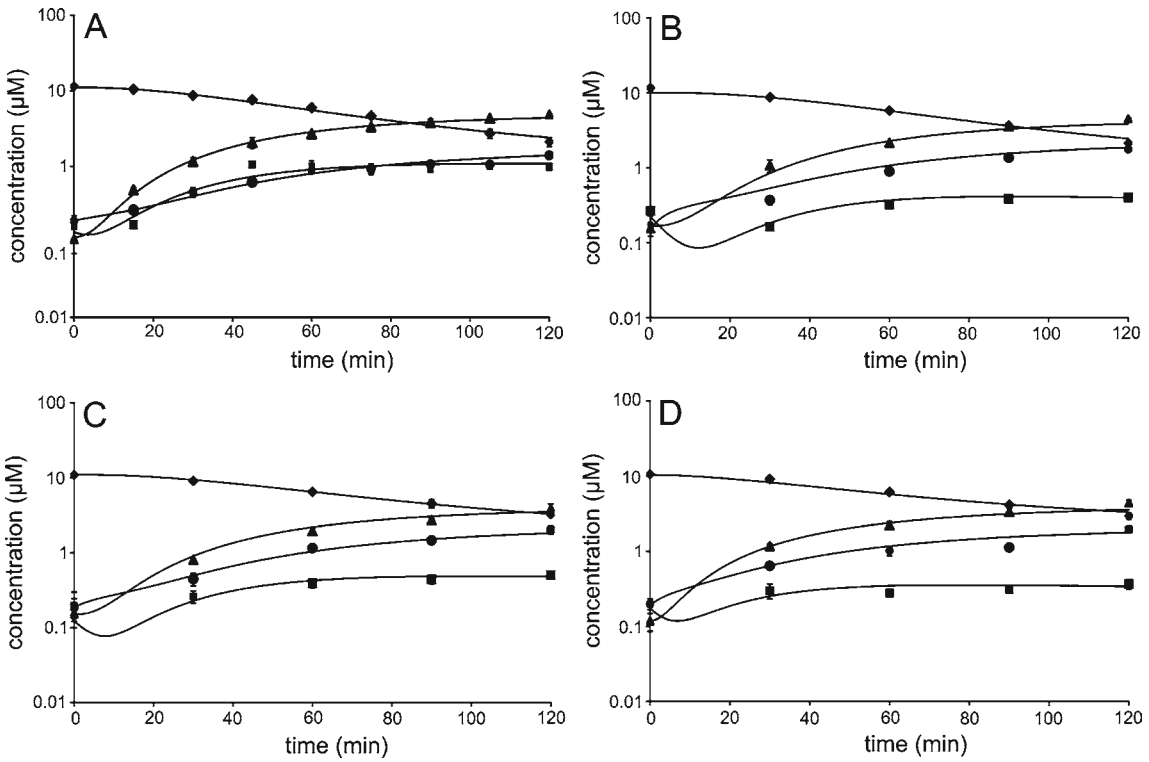

Fig. 4. Concentration-time profiles of ximelagatran (*diamonds*), ethylmelagatran (*squares*), N-hydroxymelagatran (*triangles*) and melagatran (*circles*) in hepatocyte incubations. Mean ± S.D. (n=3) and disposition model fitted curves are presented. **A** Control. **B** Co-incubation with erythromycin 50 μM. **C** Co-incubation with quinine 50 μM. **D** Co-incubation with erythromycin 50 μM and quinine 50 μM.

Table III. Result from the Simulation Study, Displayed as Obtained Percentage of Total Amount, for Investigated Efflux/Elimination Rate Relations ($k_{i\rightarrow e}/k_{met}$) and Control Simulations Without Metabolism (CTRL $_{no\ met.}$) or Distribution (CTRL $_{no\ dist.}$) of the Intermediate Metabolite. All Simulations, Except CTRL $_{no\ dist.}$, were Performed at an Influx/Efflux Rate Relation ($k_{e\rightarrow i}/k_{i\rightarrow e}$) Set to 1

		% of total amount			
		$intM_i$	$intM_e$	$intM_{tot}$	drugD
$k_{i\rightarrow e}/k_{met}$	0.1	7.6	3.7	11	37
	0.3	5.3	11	16	33
	1.0	2.1	23	25	23
	3.0	0.44	36	36	12
	10	0.25	44	44	4.7
CTRL $_{no\ met.}$		9.0	40	49	0
CTRL $_{no\ dist.}$		8.9	0	8.9	40

Values are shown for the end product (drugD) and the intermediate metabolite intracellularly ($intM_i$), extracellularly ($intM_e$) and in total ($intM_{tot}$)

that efflux rates at realistic levels, compared to the elimination rate, significantly affected the turnover of intM. A 7.9-fold decrease (from 37% to 4.7%) in drugD formation was obtained for the highest efflux/elimination rate relation compared to the lowest. Recovered drugD in control simulations, representing complete distribution of intM to the extracellular and intracellular compartments, was 0% and 40%, respectively

DISCUSSION

The major objective of this study was to investigate the metabolism of the double prodrug XIM in porcine S1 liver fractions and primary hepatocytes from pigs in the absence and presence of known inhibitors of membrane transporters. A secondary aim was to test a simple method, based on such data, for the quantitative investigation of the impact of membrane transporters on the *in vitro* disposition of metabolized drugs.

Enzyme kinetic data from S1 fractions showed that metabolism via ETM and OHM contributed to 75±4% of the total hepatic metabolism of XIM, with OHM and ETM contributing 49±3% and 25±2%, respectively. The analysis also confirmed that only 22% of the hepatic biotransformation of OHM led to the formation of MEL (12). These novel findings, together with previously reported data, strongly suggest that the hepatic metabolic scheme including only four entities is probably too simple (6). In addition, this study showed that the typical CYP inhibitors, verapamil and ketoconazole, also inhibited the esterase activity, which is consistent with another report (22). The strong inhibitory effect demonstrated in this study indicates that a clinical interaction cannot be discounted, even though therapeutic concentrations of verapamil (0.1–0.7 μM) are lower than those investigated *in vitro*. Furthermore, the complete mass balance obtained from co-incubations with verapamil also implied that the unidentified pathways involved in the metabolism of XIM and OHM were inhibited and that the loss in recovery, seen in the other incubations, was not due to any binding to the laboratory equipment.

Results from the control hepatocyte analysis suggested that intracellular, unbound concentrations of XIM and ETM were higher than extracellular concentrations, possibly caused by carrier-mediated transport processes. It is of particular interest, however, that no metabolic turnover could be detected for OHM, making a reliable determination of D_{OHM} impossible. This indicates that OHM, after formation from

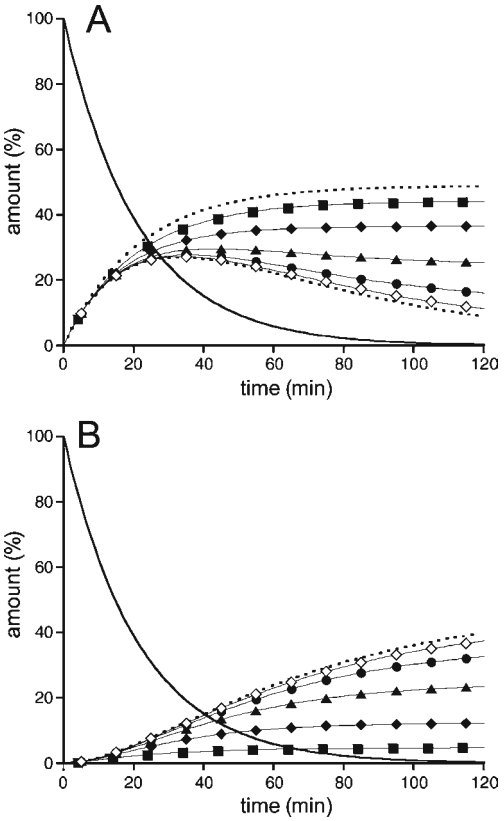

Fig. 5. Simulated concentration-time profiles of **A** intermediate metabolite and **B** end product (drugD) at investigated efflux/elimination rate relations (k_{ie}/k_{met}). k_{ie}/k_{met} = 10 (*solid squares*), k_{ie}/k_{met} = 3 (solid diamonds), k_{ie}/k_{met} = 1 (*solid triangles*) k_{ie}/k_{met}=0.3 (*solid circles*) and k_{ie}/k_{met} = 0.1 (*open diamonds*). The *solid line* represents the concentration of the double prodrug, and the *dotted lines* represent results from control simulations, i.e. maximum and minimum metabolism of the intermediate metabolite.

XIM, is rapidly transported to the extracellular space or is made inaccessible in some other way to the metabolic enzymes preventing it from being further metabolized. A deficiency in the reductase activity is unlikely, as XIM was metabolized to ETM. A high degree of association of OHM to intact intracellular organelles is also unlikely according to reports of minimal levels of binding to hepatocyte components and the absence in liver homogenate after enteral administration of XIM (7,23). The simulation study showed that reasonable rates of efflux could significantly influence the disposition of an intracellularly formed and metabolized compound. At an efflux/elimination rate ratio of 10, the turnover was reduced to 13% compared to a system with an efflux/elimination rate ratio of 0.1. However, as the simulation study was performed at a small scale, it should be emphasized that these results are not predictive for cellular systems in general. Taken together, these results suggest that the major metabolic formation pathway of MEL in the liver is via ETM. For investigation of the potential impact of membrane transporter proteins on the disposition of XIM and its metabolites, we used erythromycin and quinine as transporter inhibitors, as they showed only a minor influence on metabolism in S1 liver fractions. Membrane transporter proteins, particularly P-gp, have previously been proposed to have an impact on the hepatic disposition of XIM, MEL and perhaps some of the intermediate metabolites *in vivo* (11). Erythromycin is a well-documented inhibitor of P-gp and other membrane transporter proteins, both efflux (multidrug resistance-associated protein 1 (MRP1)) and influx (organic anion transporter 2 (OAT2) and various organic anion transporter polypeptides (OATPs)) (24–28). Quinine has been shown to have an inhibitory effect on both efflux (P-gp) and influx (organic cation transporter 1 (OCT1) and OATPs) transporters (29–31). The major effect caused by the presence of the transporter inhibitors used in this study was the increased rate of formation of MEL from ETM. We consider that the only mechanism that can provide a plausible explanation for this is interplay between membrane transporters and intracellular enzymes. If the formation of MEL is mainly dependent on the ETM pathway *in vivo*, the magnitude of altered ETM disposition may have a similar impact on the total hepatic formation of MEL. Furthermore, the distribution of OHM is likely to be independent of P-gp, as erythromycin did not affect the disposition. However, there is probably some contribution of carrier-mediated transport of OHM, as co-incubation with quinine increased the metabolic turnover enabling a reliable determination of D_{OHM}. One possible explanation for the effect of the negation of quinines by co-incubation of erythromycin is an inhibited influx of quinine, reducing the intracellular concentration. Finally, the minor effects on the disposition of XIM suggest that the hepatic disposition is independent of membrane transporter proteins inhibited by erythromycin and quinine.

It has previously been shown that primary hepatocytes are suitable for investigations of sinusoidal mechanisms (26, 32). However, the effect on canalicular transporters caused by the cell depolarization that occurs during the dispersion of cell-cell structures, including disruption of the bile ducts, has been debated (33). It has been shown that during tissue disruption, the canalicular membrane is either internalized to intracellular vesicles, integrated with the sinusoidal membrane creating a mixed outer cell membrane or localized at the cell-cell connections of couples and clusters (34,35). Reserved functionality of biliary excretion has been reported for hepatocyte couples (35). If this applies to membrane transporter proteins in general, it should be possible to detect the contribution of canaliculary drug transport with the method suggested in this study. In addition, the expression of both P-gp and MRP2 in porcine hepatocytes could be confirmed by RNA analysis, indicating the presence of these proteins. The relation between relative expression of P-gp and MRP2 was comparable with previous studies demonstrating greater levels of MRP2 than P-gp in the porcine liver (14). However, no expression of BCRP could be determined. This does not necessarily imply that BCRP was absent, as a poor primer specificity may be an issue. However, further studies focused on characterization of transport protein expression in the pig model are needed.

The level of intracellular binding, i.e. the unbound concentration (C_u) available for the enzymes, has a direct effect on the kinetics. This is problematic, as it is not practically possible to accurately determine the specific value of fraction unbound (f_u) that reflects the C_u in the very vicinity of the metabolizing enzymes. In our disposition analysis, we used the determined value of $f_{uinc.}$ for $f_{u.cell}$ to include some basic information about the level of unspecific binding in the model. As a result of this approach, the determined distribution constants (D) would also represent any discrepancies in f_u, expanding the concept of distribution to total enzymatic accessibility, including intracellular processes. However, by studying the effect of transporter protein inhibition, it is possible to distinguish the influence of carrier-mediated distribution processes. Nevertheless, there are sophisticated strategies for prediction of free fraction in a hepatocyte suspension from which it is possible to estimate the free intracellular fraction (36–39). One other potential way to estimate intracellular binding is extrapolation through ligand-complex equilibrium calculations using $f_{uinc.}$ determined in cell fractions, the protein concentration in used cell fractions and the protein concentration inside the cell. These approaches were not used, as they assume an absence of intracellular concentration gradients. Even though the information obtained with the disposition approach suggested in this study is relatively unspecific, it will still identify the dominant process for overall elimination. It is important to highlight that this method is intended and designed for metabolized drugs. Hence, we did not assess any potential role of membrane transporter proteins for the disposition of MEL. To further evaluate the utility of this approach, additional investigations will be necessary.

A straightforward evaluation of the results obtained in this study in the context of *in vivo* results from studies in pigs was complicated by the high variability of the data reported in these studies. Nevertheless, in line with results reported here, these studies indicated high biliary excretion of ETM, which was reduced by co-administration with erythromycin. Results were also in agreement regarding of the minor role played by distribution processes (biliary efflux) in the hepatic disposition of XIM and the lack of effect of erythromycin on the disposition of OHM (7). The results of this study suggest that the hepatic elimination of OHM is either extensively carried out through unidentified metabolic routes (S1 fractions) or

that it is negligible, possibly due to effective efflux mechanisms (hepatocytes). Neither of these alternatives is consistent with the published *in vivo* study that suggested high metabolic elimination to MEL and low biliary excretion (7). However, following an intravenous dose of XIM, it was also reported that OHM only represented 2% of the total plasma exposure and that the recovery of MEL only was 20% (7). These results support the theory of high biliary efflux of OHM of hepatic origin. It is also important to emphasize that the metabolism of XIM and the intermediate metabolites *in vivo* also take place in organs other than the liver, which can make interpretation less straightforward (8,9); for example, it has been reported that about 70% of absorbed doses undergo metabolic extraction in the gut wall (7).

The overall conclusions of this study were that the importance of carrier-mediated transport for the hepatic disposition of XIM in pigs is low but that it is most likely significant for the intermediate metabolites, ETM and OHM. Also, it is possible to obtain profound information about the general mechanisms that are important in the drug liver disposition with the combination of simple *in vitro* systems and disposition model proposed in this study. As primary hepatocytes are routinely used in drug discovery, this could be a suitable area of application for this approach, contributing cost-efficient information in early evaluations and decision making.

ACKNOWLEDGEMENTS

This work was supported by AstraZeneca R&D Mölndal, Mölndal, Sweden.

REFERENCES

1. Eriksson BI, Bergqvist D, Kalebo P, Dahl OE, Lindbratt S, Bylock A, et al. Ximelagatran and melagatran compared with dalteparin for prevention of venous thromboembolism after total hip or knee replacement: the METHRO II randomised trial. Lancet. 2002;360:1441–7.
2. Eriksson H, Wahlander K, Gustafsson D, Welin LT, Frison L, Schulman S. A randomized, controlled, dose-guiding study of the oral direct thrombin inhibitor ximelagatran compared with standard therapy for the treatment of acute deep vein thrombosis: THRIVE I. J Thromb Haemost. 2003;1:41–7.
3. AstraZeneca. AstraZeneca decides to withdraw Exanta™. 2006. http://www.astrazeneca.com/pressrelease/5217.aspx.
4. Scala S, Akhmed N, Rao US, Paull K, Lan LB, Dickstein B, et al. P-glycoprotein substrates and antagonists cluster into two distinct groups. Mol Pharmacol. 1997;51:1024–33.
5. Gustafsson D, Nystrom J, Carlsson S, Bredberg U, Eriksson U, Gyzander E, et al. The direct thrombin inhibitor melagatran and its oral prodrug H 376/95: intestinal absorption properties, biochemical and pharmacodynamic effects. Thromb Res. 2001;101:171–81.
6. Eriksson UG, Bredberg U, Hoffmann KJ, Thuresson A, Gabrielsson M, Ericsson H, et al. Absorption, distribution, metabolism, and excretion of ximelagatran, an oral direct thrombin inhibitor, in rats, dogs, and humans. Drug Metab Dispos. 2003;31:294–305.
7. Sjodin E, Fritsch H, Eriksson U, Logren U, Nordgren A, Forsell P, et al. Intestinal and hepatobiliary transport of ximelagatran and its metabolites in pigs. Drug Metab Dispos. 2008;36:1519–28.
8. Clement B, Lopian K. Characterization of *in vitro* biotransformation of new, orally active, direct thrombin inhibitor ximelagatran, an amidoxime and ester prodrug. Drug Metab Dispos. 2003;31:645–51.
9. Andersson S, Hofmann Y, Nordling A, Li XQ, Nivelius S, Andersson TB, et al. Characterization and partial purification of the rat and human enzyme systems active in the reduction of N-hydroxymelagatran and benzamidoxime. Drug Metab Dispos. 2005;33:570–8.
10. Bredberg E, Andersson TB, Frison L, Thuresson A, Johansson S, Eriksson-Lepkowska M, et al. Ximelagatran, an oral direct thrombin inhibitor, has a low potential for cytochrome P450-mediated drug-drug interactions. Clin Pharmacokinet. 2003; 42:765–77.
11. Eriksson UG, Dorani H, Karlsson J, Fritsch H, Hoffmann KJ, Olsson L, et al. Influence of erythromycin on the pharmacokinetics of ximelagatran may involve inhibition of P-glycoprotein-mediated excretion. Drug Metab Dispos. 2006;34:775–82.
12. Sjogren E, Lennernas H, Andersson TB, Grasjo J, Bredberg U. The multiple depletion curves method provides accurate estimates of intrinsic clearance (CLint), maximum velocity of the metabolic reaction (Vmax), and Michaelis constant (Km): accuracy and robustness evaluated through experimental data and Monte Carlo simulations. Drug Metab Dispos. 2009;37:47–58.
13. Reese JA, Byard JL. Isolation and culture of adult hepatocytes from liver biopsies. *in vitro*. 1981;17:935–40.
14. Schrickx J. ABC-transporters in the pig, Veterinary Pharmacology, Pharmacy and Toxicology. Utrecht: Universiteit Utrecht; 2006.
15. Arvidsson B, Allard E, Sjogren E, Lennernas H, Sjoberg PJ, Bergquist J. Online capillary solid phase extraction and liquid chromatographic separation with quantitative tandem mass spectrometric detection (SPE-LC-MS/MS) of ximelagatran and its metabolites in a complex matrix. J Chromatogr B Analyt Technol Biomed Life Sci. 2009;877:291–7.
16. Riley RJ, McGinnity DF, Austin RP. A unified model for predicting human hepatic, metabolic clearance from *in vitro* intrinsic clearance data in hepatocytes and microsomes. Drug Metab Dispos. 2005;33:1304–11.
17. Bayliss MK, Bell JA, Jenner WN, Park GR, Wilson K. Utility of hepatocytes to model species differences in the metabolism of loxtidine and to predict pharmacokinetic parameters in rat, dog and man. Xenobiotica. 1999;29:253–68.
18. Reinoso RF, Telfer BA, Brennan BS, Rowland M. Uptake of teicoplanin by isolated rat hepatocytes: comparison with *in vivo* hepatic distribution. Drug Metab Dispos. 2001;29:453–9.
19. Uhal BD, Roehrig KL. Effect of dietary state on hepatocyte size. Biosci Rep. 1982;2:1003–7.
20. Vom Dahl S, Hallbrucker C, Lang F, Gerok W, Haussinger D. Regulation of liver cell volume and proteolysis by glucagon and insulin. Biochem J. 1991;278(Pt 3):771–7.
21. Hallifax D, Houston JB. Uptake and intracellular binding of lipophilic amine drugs by isolated rat hepatocytes and implications for prediction of *in vivo* metabolic clearance. Drug Metab Dispos. 2006;34:1829–36.
22. Polsky-Fisher SL, Cao H, Lu P, Gibson CR. Effect of cytochromes P450 chemical inhibitors and monoclonal antibodies on human liver microsomal esterase activity. Drug Metab Dispos. 2006;34:1361–6.
23. Kenne K, Skanberg I, Glinghammar B, Berson A, Pessayre D, Flinois JP, et al. Prediction of drug-induced liver injury in humans by using *in vitro* methods: the case of ximelagatran. Toxicol *in vitro*. 2008;22:730–46.
24. Polli JW, Wring SA, Humphreys JE, Huang L, Morgan JB, Webster LO, et al. Rational use of *in vitro* P-glycoprotein assays in drug discovery. J Pharmacol Exp Ther. 2001;299:620–8.
25. Seithel A, Eberl S, Singer K, Auge D, Heinkele G, Wolf NB, et al. The influence of macrolide antibiotics on the uptake of organic anions and drugs mediated by OATP1B1 and OATP1B3. Drug Metab Dispos. 2007;35:779–86.
26. Lam JL, Okochi H, Huang Y, Benet LZ. *In vitro* and *in vivo* correlation of hepatic transporter effects on erythromycin metabolism: characterizing the importance of transporter-enzyme interplay. Drug Metab Dispos. 2006;34:1336–44.
27. Kobayashi Y, Sakai R, Ohshiro N, Ohbayashi M, Kohyama N, Yamamoto T. Possible involvement of organic anion transporter 2 on the interaction of theophylline with erythromycin in the human liver. Drug Metab Dispos. 2005;33:619–22.

28. Terashi K, Oka M, Soda H, Fukuda M, Kawabata S, Nakatomi K, et al. Interactions of ofloxacin and erythromycin with the multidrug resistance protein (MRP) in MRP-overexpressing human leukemia cells. Antimicrob Agents Chemother. 2000;44:1697–700.
29. Shitara Y, Sugiyama D, Kusuhara H, Kato Y, Abe T, Meier PJ, et al. Comparative inhibitory effects of different compounds on rat oatpl (slc21a1)- and Oatp2 (Slc21a5)-mediated transport. Pharm Res. 2002;19:147–53.
30. Zhang L, Schaner ME, Giacomini KM. Functional characterization of an organic cation transporter (hOCT1) in a transiently transfected human cell line (HeLa). J Pharmacol Exp Ther. 1998;286:354–61.
31. van der Sandt IC, Blom-Roosemalen MC, de Boer AG, Breimer DD. Specificity of doxorubicin *versus* rhodamine-123 in assessing P-glycoprotein functionality in the LLC-PK1, LLC-PK1:MDR1 and Caco-2 cell lines. Eur J Pharm Sci. 2000;11:207–14.
32. Hirano M, Maeda K, Shitara Y, Sugiyama Y. Contribution of OATP2 (OATP1B1) and OATP8 (OATP1B3) to the hepatic uptake of pitavastatin in humans. J Pharmacol Exp Ther. 2004;311:139–46.
33. Bow DA, Perry JL, Miller DS, Pritchard JB, Brouwer KL. Localization of P-gp (Abcb1) and Mrp2 (Abcc2) in freshly isolated rat hepatocytes. Drug Metab Dispos. 2008;36:198–202.
34. Gratzl R, Lassacher R, Majcen A, Graf J. Redistribution of canalicular cell membrane enzyme in hepatocytes following their isolation and during early cell culture. Hepatology. 1997;25:502–4.
35. Gautam A, Ng OC, Strazzabosco M, Boyer JL. Quantitative assessment of canalicular bile formation in isolated hepatocyte couplets using microscopic optical planimetry. J Clin Invest. 1989;83:565–73.
36. Jones HM, Hallifax D, Houston JB. Quantitative prediction of the *in vivo* inhibition of diazepam metabolism by omeprazole using rat liver microsomes and hepatocytes. Drug Metab Dispos. 2004;32:572–80.
37. Austin RP, Barton P, Mohmed S, Riley RJ. The binding of drugs to hepatocytes and its relationship to physicochemical properties. Drug Metab Dispos. 2005;33:419–25.
38. Kilford PJ, Gertz M, Houston JB, Galetin A. Hepatocellular binding of drugs: correction for unbound fraction in hepatocyte incubations using microsomal binding or drug lipophilicity data. Drug Metab Dispos. 2008;36:1194–7.
39. Lu C, Li P, Gallegos R, Uttamsingh V, Xia CQ, Miwa GT, et al. Comparison of intrinsic clearance in liver microsomes and hepatocytes from rats and humans: evaluation of free fraction and uptake in hepatocytes. Drug Metab Dispos. 2006;34:1600–5.